

Electronic structure and weak electron-phonon coupling in TaB₂

H. Rosner* and W.E. Pickett

Department of Physics, University of California, Davis, CA 95616, USA

S.-L. Drechsler, A. Handstein, G. Behr, G. Fuchs, K. Nenkov, K.-H. Müller, and H. Eschrig
Institut für Festkörper- und Werkstofforschung Dresden e.V., Postfach 270116, D-01171 Dresden, Germany
 (November 2, 2018)

We present electronic structure calculations together with resistivity, susceptibility, and specific heat measurements for TaB₂ to search for the recently contradictorily reported superconductivity and to study related normal state properties. We ascribe the absence of superconductivity down to 1.5 K for our TaB₂ samples to the generally weak electron phonon coupling derived from comparison of the calculated and measured specific heat constants. For the E_{2g} and the B_{1g} Γ point phonons we derive from the calculated deformation potentials very small electron phonon couplings for these modes, opposite to the strong coupling of the E_{2g} mode in MgB₂, probably responsible for its high T_c . In comparison to MgB₂, we discuss the origin of the quite different features in the density of states and of the Fermi surfaces. The differences are mainly due to the strong hybridization between Ta 5d and B 2p states outside the hexagonal basis plane.

74.25-q, 71.20.-b

I. INTRODUCTION

The recent discovery of superconductivity in MgB₂ [1] has initiated an immediate broad research activity due to the surprisingly high transition temperature $T_c \sim 40$ K in a seemingly ordinary $s-p$ metal. Investigation of related $s-p$ diborides MB₂ (M = Li, Be, Al) [2–4] and a series of isostructural transition metal diborides (M = Sc, Ti, Zr, Hf, V, Ta, Cr, Mo, Nb) [5–7] has shown that only few of them seem to be superconducting, and then only at very low temperatures. Since the understanding of the pairing mechanism in MgB₂ is still in its early stages, a study of the isomorphous compounds with low transition temperatures or with absence of superconductivity, respectively, could be helpful in clarifying the expected very substantial electronic differences.

Contradictory reports about superconductivity in TaB₂ have appeared; one found superconductivity at $T_c \sim 9.5$ K, [8,9] while another found no superconductivity down to 4.4 K. [10] TaB₂ is isovalent with NbB₂, where the occurrence of superconductivity, or at least the value of T_c , is likewise uncertain. NbB₂ was reported to be superconducting at 3.87 K, [6] superconducting only at 0.62 K, [7] and not superconducting above 0.37 K. [10] Clearly there is sample dependence for both TaB₂ and NbB₂, and no doubt for many other diborides as well.

In an attempt to begin to settle some of these discrepancies, we address TaB₂ specifically in this paper with a joint theoretical (Secs. II A and III A) and experimental (Secs. II B, III B) investigation. In Sec. III we provide an analysis of its electronic structure, and contrast it with that of MgB₂. We also present specific heat, susceptibility as well as resistivity data for two almost single phase samples. One of them exhibited a significant amount of boron vacancies.

II. METHODS

A. Band structure calculations

We calculated the electronic structure of TaB₂ in the hexagonal space group (SG) P6₃/mmc (No. 191) with the lattice constants $a = 3.082$ Å and $c = 3.243$ Å. [8] The frozen phonon calculations for the E_{2g} and B_{1g} modes were done in the orthorhombic SG Cmmm (No. 65) and in the trigonal SG P $\bar{3}$ m1 (No. 164), respectively.

Our band structure calculations were performed using the full-potential nonorthogonal local-orbital minimum-basis scheme (FPLO) [11] within the local density approximation (LDA). In these scalar relativistic calculations we used the exchange and correlation potential of Perdew and Zunger. [12] Ta 5s, 5p, 6s, 6p, 5d states and B 2s, 2p, 3d, were chosen as minimum basis set for the valence states. All lower lying states were treated as core states. The inclusion of the relatively extended Ta 5s, 5p semi-core states as band states was done because of the considerable overlap of these states on nearest neighbors. This overlap would be neglected if they were treated as core states in our FPLO scheme. Accounting for this overlap is of importance especially for the calculations of phonon frequencies that we report. B 3d states were added to allow for boron polarizability. The spatial extension of the basis orbitals, controlled by a confining potential [13] $(r/r_0)^4$, was optimized to minimize the total energy. The self-consistent potentials were carried out on a k -mesh of 20 k -points in each direction of the Brillouin zone, which corresponds to 481, 784 and 1221 in irreducible part for P6₃/mmc, P $\bar{3}$ m1, and Cmmm SG, respectively. Our FPLO approach has been proved by recent comparison to FLAPW results in many cases to have an absolute accuracy of 1mHartree/atom for the

total energy and a much higher accuracy for the relative total energy changes.

B. Sample preparation and measurements

Two different TaB_2 samples, one with near stoichiometric and one with boron deficient compositions, were prepared starting from the pure elements Ta ($> 99.9\%$) and B ($> 99.9\%$) by arc melting furnace under purified argon atmosphere. To ensure a better homogeneity the samples were turned several times. The phase content was checked by X-ray diffraction (XRD) using Co-K α radiation.

The samples contain the hexagonal AlB_2 phase mainly, 95% in sample No. 1 and 97% in sample No. 2. In both samples small amounts ($< 5\%$) of a second phase were found which are B for sample No. 1 and Ta_3B_4 for sample No. 2. The compositions of the main phases measured by electron probe microanalysis in the WDX modus showed a composition of about $\text{TaB}_{2.03}$ (sample No. 1) and compositions of $\text{TaB}_{1.29}$ (sample No. 2).

Furthermore, the XRD resulted in quite different lattice parameters for the two samples ranging from $a = 3.098 \pm 0.002$ nm and $c = 3.224 \pm 0.003$ Å of the B-deficient sample to $a = 3.067 \pm 0.002$ Å and $c = 3.286 \pm 0.006$ Å of the B-rich sample.

The specific heat of both TaB_2 samples was measured in the temperature range between 2 and 16 K using a Quantum Design PPMS relaxation calorimeter. The addenda which were determined in a separate run were subtracted in order to obtain the specific heat data for TaB_2 .

Magnetization measurements have been performed using a Quantum Design-SQUID magnetometer in the temperature range down to 1.8 K. Resistivity measurements down to 1.5 K have been performed using the standard four point method.

III. RESULTS AND DISCUSSION

A. Theoretical results

In Figure 1 we display the total as well as the atom decomposed density of states (DOS) of TaB_2 . The B $2p$ and Ta $5d$ states share almost equally in the occupied valence bands in the region -10 to -2 eV (the Fermi level $E = \varepsilon_F$ is taken as the zero of energy). Our DOS is in agreement with that of P.P. Singh [14], which we became aware right after the completion of our study.

A striking difference in comparison to MgB_2 is the dominating contribution of Ta $5d$ states to the DOS at Fermi level, which contribute about 70% of the total DOS; in MgB_2 the DOS at Fermi level is dominated by B- $2p$ states (see Figure 2 for comparison [15]). Although a rigid band picture is very limited in this case, a valence analysis shows that due to the 3 additional valence

electrons of Ta with respect to Mg, the Fermi level has shifted from the bonding B states below the hybridization gap in MgB_2 to the anti-bonding states above this gap in TaB_2 . From the very similar shape of the partial B and Ta DOS, a strong hybridization between B $2p$ and Ta $5d$ states is obvious, mentioned below in more detail.

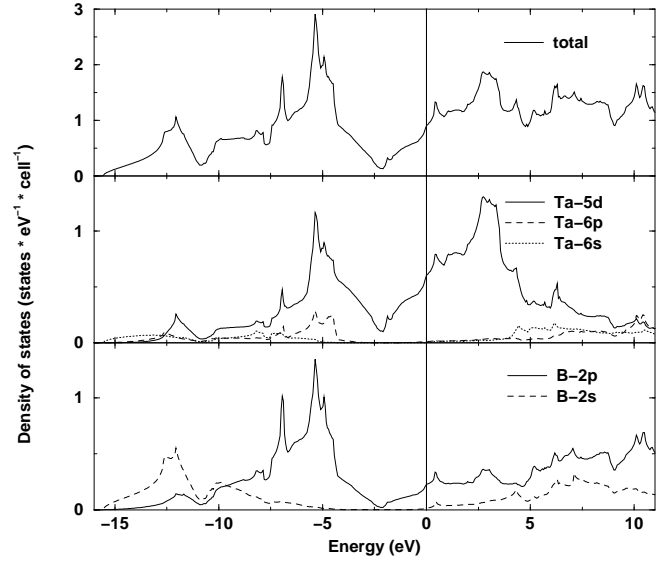


FIG. 1. Total DOS and partial DOS of TaB_2 . The upper panel gives the total DOS, the middle and the lower panels show the contribution of Ta and B, respectively. The Fermi level is at zero energy.

The calculated value of the density of states at the Fermi level $N(\varepsilon_F)$ is slightly higher for TaB_2 ($N(\varepsilon_F) = 0.91$ states/(eV \times cell)) than for MgB_2 ($N(\varepsilon_F) = 0.71$ states/eV \times cell), in agreement with Refs. [16,17]. This corresponds to a bare specific heat coefficient $\gamma_0 = 2.14$ mJ/(mole \times K 2) for TaB_2 .

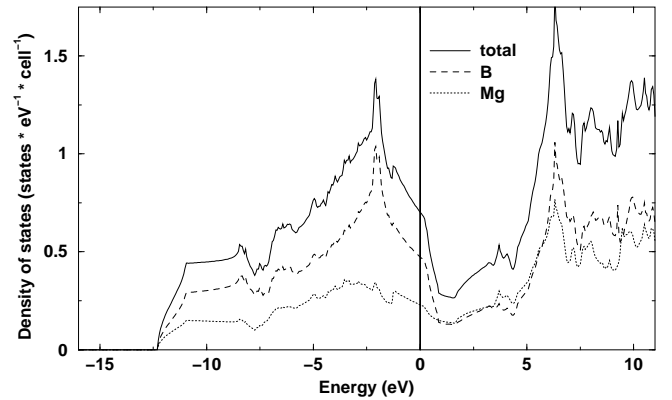


FIG. 2. Total DOS and partial DOS of MgB_2 . The partial DOS are calculated by projection to the minimum orbital basis. The Fermi level is at zero energy.

Figure 3 shows the band structure of TaB_2 along the symmetry lines of the hexagonal cell. As already men-

tioned above, the bonding B σ states, which lie in the region -10 eV to -2 eV and are highlighted in the middle panel, are completely filled. These states, which are unoccupied along the Γ -A direction in MgB_2 (compare to Figures 1 of Refs. [16,17]), lie now between -5 eV and -2 eV for this symmetry line and show almost 3 eV dispersion along the hexagonal axis (Γ -A) compared to 0.6 eV in MgB_2 . The two-dimensional character of these states in MgB_2 is obviously destroyed in TaB_2 . Furthermore, we find around the A-L-H plane of the k -space a strong hybridisation of those B σ states with the Ta $5d_{xz}$ and $5d_{yz}$ states, indicated in the lower panel of Figure 3. Once more we like to emphasize the difference to MgB_2 , where these states are of nearly pure B σ character.

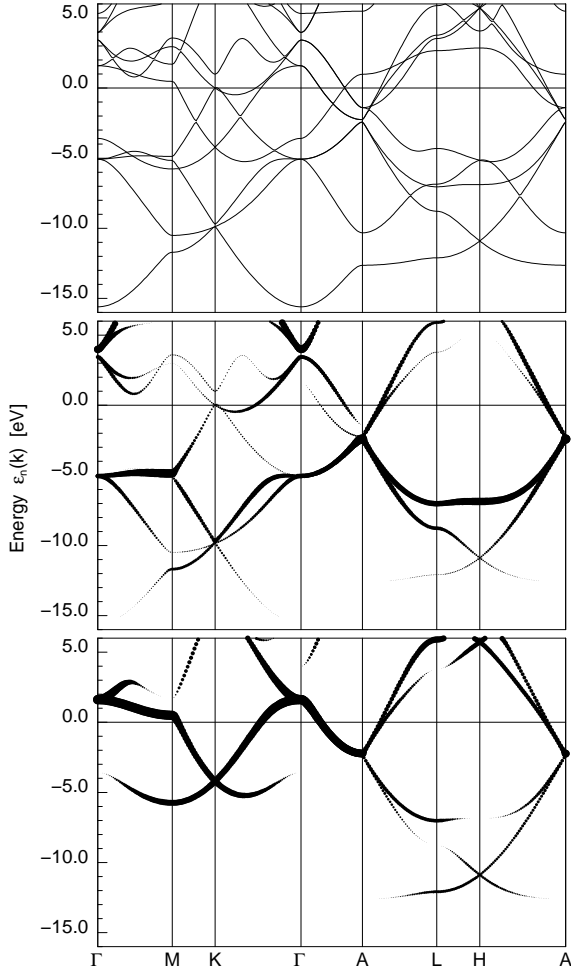


FIG. 3. Band structure and band characters of TaB_2 . The middle and the lower panels show the band characters of the B $2p_{x,y}$ orbitals and the Ta $5d_{xz,yz}$ orbitals, respectively. The line width is scaled with the orbital weights of the corresponding orbitals.

The corresponding Fermi surface (FS) of TaB_2 is shown in Figure 4. For convenience of comparison with MgB_2 (compare to Fig. 3 in Ref. [17]), we have chosen the A point as the center of the hexagonal prism. All three

sheets of the FS of TaB_2 are electron-like. Because of the strong dispersion of the antibonding B σ - Ta $5d_{xz,yz}$ states, they build closed FS around the A point (see middle and lower panel of Fig. 4), where the hole-like quasi two-dimensional tubes are found in MgB_2 . The large FS in the upper panel of Fig. 4 is due to Ta $5d$ states, the contribution of B states to this sheet is almost negligible.

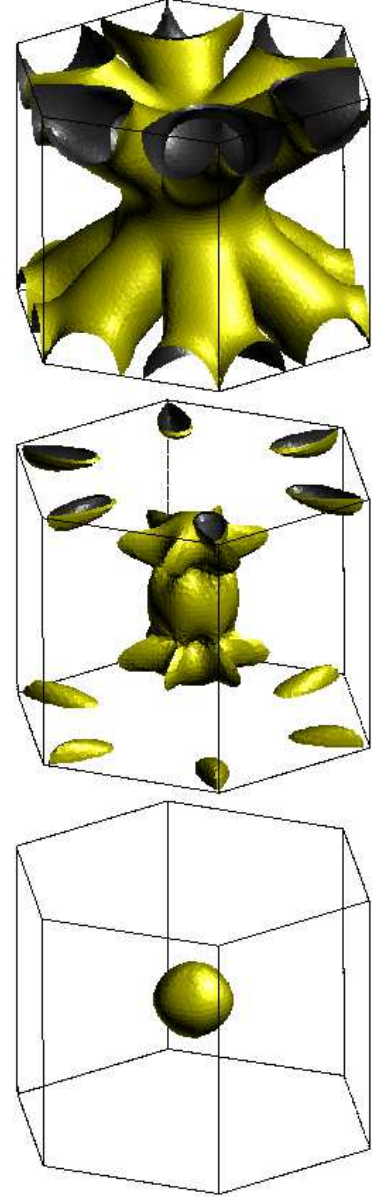


FIG. 4. The three different sheets of the Fermi surface of TaB_2 , all sheets are electron-like. The A point corresponds to the center of the hexagonal prism, the Γ point is the midpoint of the lower and upper hexagon.

To account for the experimental uncertainty in the lattice constants for different samples [18], we also investigated the influence of different lattice constants for the experimentally reported range on the electronic struc-

ture. The changes for the relevant features in the band structure are negligible, the DOS is basically unchanged, $N(\varepsilon_F)$ varies by less than 2%.

For a rough estimate of the electron-phonon (el-ph) coupling in TaB₂, we calculated the phonon frequencies and the deformation potential of the E_{2g} (in-plane displacement of the borons) and the B_{1g} (borons displaced along z in different directions) zone-center phonon modes. Their frequencies are 98 meV and 85 meV, respectively. For the corresponding frequencies in MgB₂ Kortus *et al.* [17] reported 58 meV and 86 meV, respectively. For AlB₂ 118 meV and 60 meV, respectively, were calculated. [19] Already from the strong hardening of the calculated E_{2g} frequency compared with MgB₂ one can conclude a strongly reduced electron phonon coupling of this mode.

Figure 5 shows the calculated band structure for the frozen E_{2g} phonon mode of TaB₂ with a B displacement of $\Delta u_B = 0.018$ Å. The B bond stretching mode splits the antibonding B σ -Ta 5d_{xz,yz} bands along the Γ -A line. For an averaged split $\Delta\varepsilon_k/\Delta u_B \sim 9$ eV/Å we find a deformation potential $D_{E_{2g}} \sim 4.5$ eV/Å about 3 times smaller than $D_{E_{2g}}$ in MgB₂. [16] Calculating larger elongations up to the actual rms we found a nearly linear dependence of the deformation potential $D_{E_{2g}}$ on the elongation Δu .

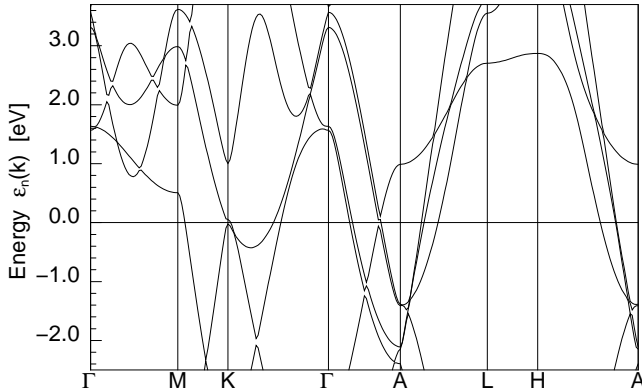


FIG. 5. Band structure for frozen E_{2g} mode, plotted along the same lines as in Fig. 3 to facilitate comparison. The two-fold degenerate bands in Fig. 3, crossing the Fermi level along the Γ -A direction, are split due to the symmetry reducing phonon mode.

Following Ref. [16], we can estimate the coupling from this mode alone using Eq. (2.34) of Kahn and Allen [20] for the EP matrix element in terms of $D_{E_{2g}}$. With $N_{E_{2g}}(\varepsilon_F) = 0.28$, resulting from a summation of the calculated orbital projected DOS for the orbitals mainly involved in the deformed band, we find

$$\lambda_{E_{2g}} = N_{E_{2g}}(\varepsilon_F) \left[\frac{\hbar}{2M_B \omega^2} \right] \left| \sum_{j=1,2} \hat{\varepsilon}_j D_j \right|^2 \sim 0.055. \quad (1)$$

The sum on j runs over the two B atoms of the E_{2g} mode, for M_B we used the isotope averaged mass of B.

Due to the high frequency ω and the smaller deformation potential $D_{E_{2g}}$, we get a coupling smaller by a factor of about 20 compared to MgB₂.

From a corresponding calculation of the coupling constant for the B_{1g} mode, reported [19] to be softened in AlB₂ ($\omega = 60$ meV), we find an even slightly smaller contribution compared with the already weak coupled E_{2g} phonon.

Assuming similar coupling to the acoustic phonons as reported [19] for MgB₂ or AlB₂ and comparable contributions of other modes, the total el-ph coupling constant might be no more than $\lambda \sim 0.2$.

B. Experimental results

The results of the specific heat measurements are shown in Figure 6. Since no superconductivity was observed at least in the temperature range down to 1.8 K from magnetization measurements (see Figure 7), and down to 1.5 K from resistance measurements (see Figure 8), the results of the specific heat measurements are shown in the c_p/T vs. T^2 plot. Thus, assuming standard normal metal behaviour, the Sommerfeld coefficient γ was determined using the relation

$$c_p/T = \gamma + \frac{12}{5} R \pi^4 \Theta_0^{-3} T^2, \quad (2)$$

where R being the ideal gas constant and Θ_0 the initial Debye temperature.

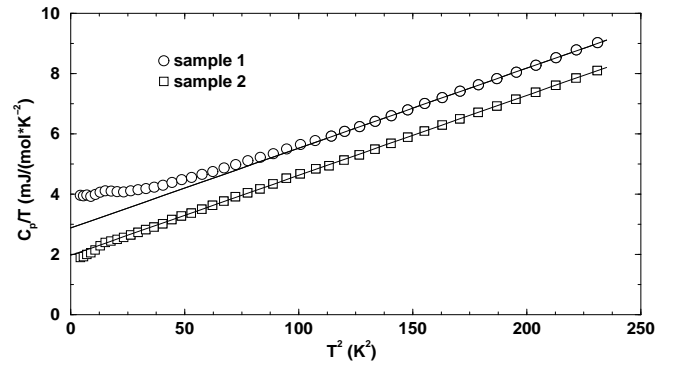


FIG. 6. Specific heat $c_p(T)/T$ versus T^2 of two TaB₂ samples at zero magnetic field. The lines correspond to linear regression fits of the experimental data for temperatures $T > 8$ K (sample 1) and $T > 4$ K (sample 2), respectively.

The investigated TaB₂ samples show distinct anomalies at temperatures around 4 K which are, however, not due to superconductivity as was found from magnetization and resistance measurements.

Sizable deviations from the linear fits, shown in Figure 6 are observed especially for sample No. 1. Similar deviations as found for these two samples are known as well from MgB₂ [21–23]. Since such anomalous contributions do not essentially change in the superconducting state of

MgB₂, we ascribe them to lattice effects related to boron disorder present in all diborides.

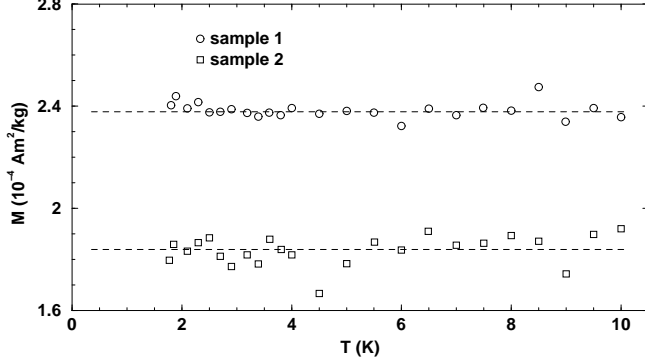


FIG. 7. Temperature dependent magnetization M of two TaB₂ samples in the temperature range $1.8 \text{ K} < T < 10 \text{ K}$ at an applied magnetic field of $H = 10 \text{ Oe}$.

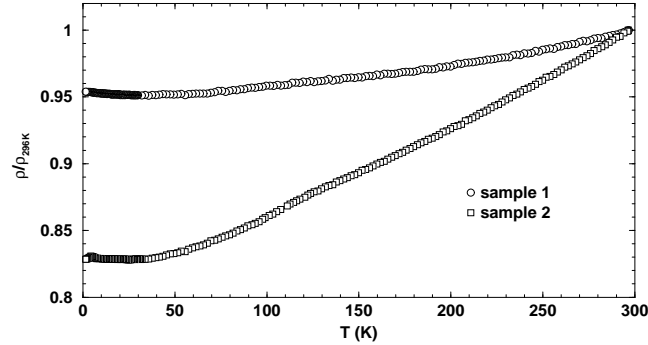


FIG. 8. Temperature dependence of the resistivity normalized to its values $\rho_{296\text{K}} = 350 \mu\Omega\text{cm}$ (sample 1) and $\rho_{296\text{K}} = 199 \mu\Omega\text{cm}$ (sample 2) at $T = 296 \text{ K}$ in the temperature range $1.5 \text{ K} < T < 296 \text{ K}$.

Naturally, the initial Debye temperature $\Theta_0 \approx 417 \pm 2 \text{ K}$ is smaller than the corresponding value reported for MgB₂ of 750 to 800 K [24,22,21]. But it is somewhat *harder* than the value one might expect from a simple scaling with the square root of the total mass ratio: $369 \pm 11 \text{ K}$. This is in line with the hardening calculated for the optical phonons at the γ -point as reported above.

TABLE I. Experimental results: Specific heat (Sommerfeld constant γ , (column 2), Debye energy Θ_0 (column 3), residual resistivity ratio RRR (column 4), and resistivity $\rho_{296\text{K}}$ at $T = 296 \text{ K}$.

Sample No.	γ [mJ /mol K ⁻²]	Θ_0 [K]	RRR	$\rho_{296\text{K}}$ $\mu\Omega\text{cm}$
1	2.8	415	1.05	350
2	2.0	419	1.2	199

The theoretically estimated value of the el-ph coupling constant λ is in accordance with those small λ values derived by comparing the experimental value of the Sommerfeld constant (see figure 6) with the calculated DOS at the Fermi level $N(\varepsilon_F)$

$$\gamma_{exp} = (\pi^2/3)k_B^2(1 + \lambda)N(\varepsilon_F) = \gamma_0(1 + \lambda). \quad (3)$$

Using our calculated $\gamma_0 = 2.14 \text{ mJ/mole} \times \text{K}^2$ and the measured $\gamma_{exp} = 2.8 \text{ mJ/mole} \times \text{K}^2$ of sample No. 1, we obtain an empirical value of $\lambda_{No. 1} = 0.3$. If this estimate is correct, a sizable contribution of relatively low-frequency phonons involving Ta-vibrations can be expected.

The low value of $\gamma_{exp} = 2 \text{ mJ/mole} \times \text{K}^2$ for sample No. 2 can be ascribed to the significant number of boron vacancies in understoichiometric TaB_{2- δ} samples. Within a very crude estimate, supposing a rigid band behaviour and using the atomic partial density of states $N_{Ta}(\varepsilon_F)$ and $N_B(\varepsilon_F)$ (see Figure 1) we assume for the effective bare specific heat constant $\gamma_{0,eff}$

$$\gamma_{0,eff} < (\pi^2/3)k_B^2(N_{Ta}(\varepsilon_F) + (2 - \delta)N_B(\varepsilon_F)). \quad (4)$$

For TaB_{1.29} (sample No. 2) this yields $\gamma_{0,eff} = 1.8986$ corresponding to $\lambda_{No. 2} = 0.053$. Considering additionally broadening effects in the DOS due to disorder in the vacancy distribution and other impurities, that λ value can be taken as a lower bound.

Adopting a standard value of the Coulomb pseudopotential $\mu^* = 0.13$ one arrives at negligible values of the transition temperature $T_c \sim 10^{-7} \text{ K}$, irrespectively of the details of the shape of the Eliashberg function, i.e. the averaged phonon frequency. If even the pseudo potential μ^* would be ignored, T_c would not exceed 18 mK. Thus, the experimental evidence for the absence of superconductivity, possibly even down to several 100 mK, [5] becomes very plausible already in the traditional electron-phonon Migdal-Eliashberg picture.

IV. CONCLUSIONS

Although TaB₂ occurs in the same crystal structure as MgB₂, it should not be considered as a close relative of MgB₂ with respect to the electronic structure (even if it would be found superconducting at very low temperatures). The major differences occur due to: (i) the different band filling because of the three additional valence electrons of Ta with respect to Mg, resulting in a shift of the the Fermi level from the bonding B- σ states in MgB₂ to the antibonding B- σ - Ta- d hybrid states in TaB₂, (ii) the strong out of plane hybridization of the B $2p$ states with Ta, (iii) the weak electron phonon coupling, especially of the E_{2g} mode, which is strongly coupled in MgB₂.

According to our experimental results, TaB₂ is not superconducting down to 1.5 K. Thus, we confirm the earlier results of Refs. [10,5] and disprove at the same time

the speculation about superconductivity around 9.5 K reported in Ref. [8]. Because in our opinion the main reason for the absence of superconductivity in TaB₂ is the different position of the Fermi level (with respect to MgB₂), huge hole doping might “reintroduce” superconductivity at relatively high temperatures.

In other words, the results obtained here suggest that the empirical absence or low-temperature superconductivity established in many transition metal (or rare earth) diborides with *electrons* as the potentially paired charge carriers, stressed by Hirsch [25], might be explained in the traditional electron-phonon picture simply by a *weak* electron-phonon interaction. In that case there is no need to explain this behavior by the absence of a sophisticated Coulomb interaction driven non-phonon mechanism which works exclusively for holes [25].

Corresponding studies for other related transition metal diborides of experimental interest will be published elsewhere.

V. ACKNOWLEDGMENTS

We thank J.M. An and S.V. Shulga for discussions and N. Mattern for providing us with the XRD-data. This work was supported by the DAAD (individual grant H.R.), the ONR Grant No. N00017-97-1-0956, the SFB 463, and the Deutsche Forschungsgemeinschaft.

* Corresponding author: helge@physics.ucdavis.edu

- [1] J. Nagamatsu, N. Nakagawa, T. Muranaka, Y. Zenitani, and J. Akimitsu, *Nature*, **410**, 63 (2001).
- [2] J.S. Slusky, N. Rogado, K.A. Regan, M.A. Hayward, P. Khalifah, T. He, K. Inumaru, S. Loureiro, M.K. Haas, H.W. Zandbergen, and R.J. Cava, *cond-mat/0102262*, (2001).
- [3] I. Felner, *cond-mat/0102508* (2001).
- [4] Y.G. Zhao, X.P. Zhang, P.Y. Qiao, H.T. Zhang, S.L. Jia, B.S. Cao, M.H. Zhu, Z.H. Han, X.L. Wang, and B.L. Gu, *cond-mat/0104063*, (2001).
- [5] G.V. Samsonov and I.M. Vinitsky, *Refractory Compounds (in Russian)*, Metallurgia, Moskva, (1976).
- [6] A.S. Cooper, E. Corenzerst, L.D. Longinotti, B.T. Matias, and W.H. Zachariasen, *Proc. Natl. Acad. Sci.* **67**, 313 (1970).
- [7] L. Leyarovska and E. Leyarovski, *J. Less-Common Metals*, **67**, 249 (1979).
- [8] D. Kaczorowski, A.J. Zaleski, O.J. Zogal, J. Klamut, *cond-mat/0103571* (2001).
- [9] D. Kaczorowski, J. Klamut, A.J. Zaleski, *cond-mat/0104479* (2001).
- [10] V.A. Gasparov, N.S. Sidorov, I.I. Zver'kova, M.P. Kulakov, *cond-mat/0104323* (2001).
- [11] K. Koepernik and H. Eschrig, *Phys. Rev. B* **59**, 1743 (1999).
- [12] J. P. Perdew and A. Zunger, *Phys. Rev. B* **23**, 5048 (1981).
- [13] H. Eschrig, *Optimized LCAO Method and the Electronic Structure of Extended Systems* (Springer, Berlin, 1989).
- [14] P.P. Singh, *cond-mat/0104580* (2001).
- [15] Our band structure calculations for MgB₂ are in excellent agreement with those of Refs. [16,17]. The partial DOS naturally differ from Ref. [17] because of different calculational methods. To calculate the partial DOS, we use the projection onto our minimal basis set instead of a projection onto muffin tin spheres in Ref. [17], which finds a large contribution of the interstitial plane wave region.
- [16] J.M. An and W.E. Pickett, *Phys. Rev. Lett.* **86**, 4366 (2001).
- [17] J. Kortus, I.I. Mazin, K.D. Belashchenko, V.P. Antropov, and L.L. Boyer, *Phys. Rev. Lett.* (to be published)
- [18] The published lattice constants for TaB₂ scatter much stronger than the usual experimental errors in an XRD experiment. We found parameter sets reported with $3.057 \text{ \AA} < a < 3.0966 \text{ \AA}$ and $3.224 \text{ \AA} < c < 3.288$. [26,10,27] The different lattice constants are most probably due to different B contents of different samples.
- [19] K.-P. Bohnen, R. Heid, and B. Renker, *Phys. Rev. Lett.*, (to be published), *cond-mat/0103319* (2001).
- [20] F.S. Kahn and P.B. Allen, *Phys. Rev. B* **29**, 3341 (1984)
- [21] Y. Wang, T. Plackowski, and A. Junod, *Prep. cond-mat/* (2001)
- [22] R.K. Kremer, B.J. Gibson, and K. Ahn, *cond-mat/0102432* (2001).
- [23] E. Bauer, Ch. Paul, St. Berger, S. Majumdar, H. Michor, M. Giovannini, A. Saccone, and A. Bianconi, *J. of Phys.: Condens. Matter* **13**, L487 (2001).
- [24] S.L. Bud'ko et al. *PRL* **86**, 1877 (2001).
- [25] J.E. Hirsch, preprint *cond-mat/0102115 v3* (2001).
- [26] P. Villars and L.D. Calvert, “Pearson’s Handbook of Crystallographic Data for Intermetallic Phases” vol. 2, pp. 16939-16940, The Materials Information Society, Materials Park, OH 44073, Library of Congress Cataloging in Publication Data (1991).
- [27] S. Otani, M.M. Korsukova, and T. Mitsuhashi, *J. of Crystal Growth* **194**, 430 (1998).